Sachs, Malte; Karttunen, Antti J.; Kraus, Florian

Half-metallicity in uranium intermetallics

Published in:
Journal of Physics Condensed Matter

DOI:
10.1088/1361-648X/aaeeca

Published: 16/01/2019

Document Version
Peer-reviewed accepted author manuscript, also known as Final accepted manuscript or Post-print

Half-metallicity in uranium intermetallics: Crystal structure prediction of a high-pressure phase of UCo

Malte Sachs[a], Antti J. Karttunen[b], Florian Kraus[a]*

[a]*Fachbereich Chemie, Philipps-Universität Marburg, Hans-Meerwein-Straße 4, 35032 Marburg, Germany*

[b]*Department of Chemistry and Materials Science, Aalto University, Kemistintie 1 FI-02150 Espoo, Finland*

Corresponding author address:
Name: Florian Kraus
Philipps-Universität Marburg, Fachbereich Chemie
Hans-Meerwein-Straße 4, 35032 Marburg, Germany
Mail: f.kraus@.uni-marburg.de
Telefon: +49 6421 28 – 26 66 8

Abstract

Evolutionary crystal structure prediction methods combined with Density Functional Theory (DFT) calculations reveal a high-pressure (hp) phase of the intermetallic compound UCo crystalizing in the NaTl structure type ($Fd\bar{3}m, cF16$). We predict this compound to be formed at pressures below 9 GPa. Hp-UCo shows the same structural trends as the two experimentally known pseudo-binary compounds $UCo_{0.2}Rh_{0.8}$ and $UNi_{0.8}Pt_{0.2}$. We classify them as ordered solid solutions of a bcc lattice following *Vegard's* law. We predict hp-UCo and its adjacent phases UFe and UNi to be itinerant magnets. In the limit of vanishing spin-orbit interactions UFe and hp-UCo are half-metallic ferrimagnets. Spin-orbit coupling generally reduces the spin-polarization at the Fermi level. In case of hp-UCo the decrease depends on the applied DFT functional making the prediction of actual occurrence of half-metallicity problematic. In case of UFe the results are less dependent on the DFT functional. We demonstrate with these calulations that against "common sense" also materials with heavy elements can be interesting candidates for half-metallicity. We highlight that the NaTl structure type should be an interesting candidate for further investigations of half-metallicity.

1. Introduction

Substantial scientific effort was spent during the past decades investigating uranium containing intermetallic compounds because of the remarkable properties of the uranium 5f electrons.[1–3] These electrons are generally discussed to lie on a border between itinerant and localized behavior. By alloying uranium with other metals, it is possible to push the properties of the 5f electrons in the one or the other direction. This results in a rich diversity of interesting phenomena in uranium containing intermetallics including low-symmetry crystal structures (e.g. ß-U[4], UCo[5], UIr[6]), charge-density waves (e.g. α-U[7,8]), itinerant magnetism (e.g. UFe_2[9], UIr[10]), conventional superconductivity (e.g. U_6T, *T:* Mn, Fe, Co, Ni)[11,12], heavy fermion superconductivity (e.g. UBe_{13}[13], UPt_3[14], URu_2Si_2[15]) as well as ferromagnetic superconductivity in UGe_2.[16]

With this report we want to add another fascinating property to the compound class of uranium intermetallics: half-metallicity. Half-metals are characterized by only one spin channel to be metallic.[17,18] The valence and conduction bands of the other spin channel are separated by an energy gap. The Fermi level E_F lies within this gap resulting in a 100 % spin-polarization at E_F for these compounds. However, 100 % spin-polarization is a hypothetical situation that holds only in the limit of vanishing temperature and neglecting spin-orbit interactions.[18] Therefore, it is kind of "common sense" that the strong spin-orbit interactions expected for heavy elements should destroy half-metallicity. However, it is suggested that in suitable space groups, which allow for the proper band symmetry, half-metallicity can persist even in case of strong spin-orbit interactions.[19]

Investigating the binary phase diagrams of uranium with the iron and platinum metals *T*: Fe, Co, Ni, Rh, Ir, Pd, Pt reveals that only cobalt, iridium and platinum form compounds of the composition U*T*.[20] UCo crystalizes in an individual structure[5] type at room temperature that can be described as a strongly distorted CsCl type structure[21] as shown in Figure 1a,b. Because of its peculiar crystal structure, we found UCo to be an interesting candidate for testing Density Functional Theory (DFT) based crystal structure prediction. The evolutionary algorithm USPEX[22–24] has proven its applicability in this area by correctly predicting several high-pressure phases[25,26] as well as entire phase diagrams.[27] Applying the USPEX algorithm to the binary alloy UCo we find a possible high-pressure (hp) phase of this compound crystalizing in the NaTl structure type (Figure 1c). We will show in this paper that hp-UCo and its alloys with the iron metals display half-metallic properties and thus want to demonstrate that also compounds with *heavy* elements can be interesting candidates for half-metallicity.

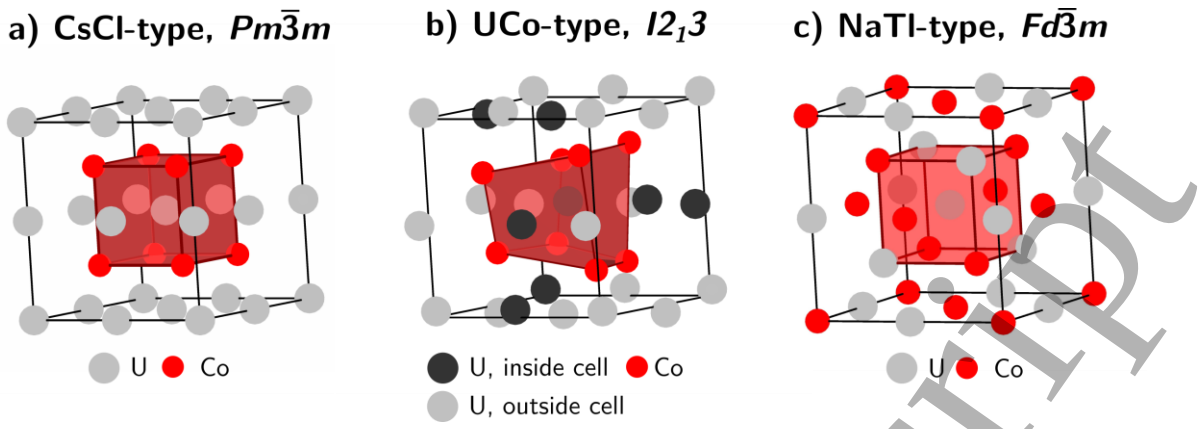

Figure 1: Sections of the crystal structure of UCo crystallizing in **a)** the CsCl structure type, **b)** the UCo structure type and **c)** the NaTl structure type. The coordination polyhedron of the central uranium atom is emphasized in each picture.

2. Computational Details

We performed total energy calculations and structural optimizations in the framework of DFT using the software package *Quantum Espresso*[28,29] version 6.2 that is based on plane-waves and pseudopotentials. We employed the GGA-PBE[30] and LDA-PW[31] exchange-correlation functional and projector augmented wave (PAW)[32] pseudopotentials. We further performed LDA+*U* calculations using the rotationally invariant scheme of Liechtenstein and coworkers[33] with the fully localized limit (FFL) double counting correction as implemented in *Quantum Espresso*.[28,29] As not stated otherwise, we applied an effective Coulomb and exchange interaction of $U = 1.5$ eV and $J = 0.5$ eV, respectively.

We used scalar relativistic as well as full relativistic PAWs to account for spin-orbit coupling (SOC). In case of the d-elements *T*: Fe, Co, Ni, Rh, Ir we used pseudopotentials from the pslibrary.[34] To model mixed occupations on the transition metal sides, we followed the concepts of the virtual crystal approximation (VCA) approach and constructed pseudopotentials with odd core-charge and interpolating the pseudopotential parameters by the ones of the adjacent elements. In case of uranium, we constructed optimized PAWs using the *atomic* code distributed with the *Quantum Espresso* package. The uranium PAWs include the 6s and 6p semi-core states and two projectors per angular momentum channel. The detailed setup for the generation of the uranium PAWs as well as benchmark results are given in Table S1, Table S2 and Figure S1.

The calculations were performed using a 75 Ry kinetic-energy and a 600 Ry charge-density cutoff, a Marzari-Vanderbilt cold smearing of 0.01 Ry and a centered 20x20x20 k-points grid with respect to the bcc cells. For larger cells the k-points grids were reduced to maintain the same reciprocal cell resolution. These settings enable a total energy convergence of < 1 mRy and a stress convergence of < 1 kbar.

Structural relaxations were performed using the scalar relativistic PAWs. Bulk moduli B_0 were calculated by fitting the volume dependency of the total energy to the Murnaghan equation of state (Eq. 1):

$$E(V) = E_0 + B_0 \frac{V}{B'_0}\left(\left(\frac{V_0}{V}\right)^{B'_0}\frac{1}{B'_0 - 1} + 1\right) - B_0 \frac{V_0}{B'_0 - 1} \quad (1)$$

where E_0, V_0, B_0, and B'_0 are the total energy, the volume, the bulk modulus, and the pressure derivative of the bulk modulus at zero pressure, respectively. For the Murnaghan-fits, a series of single-point calculations at different unit cell volumes were performed by keeping the atomic positions and the axis-ratios constant. For these calculations full relativistic PAWs including spin-orbit coupling were used. The enthalpies of formation ΔH_f were calculated at 0 K. Their pressure dependency was derived from the energies of the fitted Murnaghan equation of states.

The phonon dispersion and phonon density of states of hp-UCo were calculated at 0 GPa in the framework of Density-Functional Perturbation Theory (DFPT) using the program *PHonon* as implemented in the *Quantum Espresso* software package.[35] The calculations were performed using the GGA functional, spin-polarization (sp), scalar relativistic PAWs and a 2x2x2 grid of q-points. Acoustic Sum Rule correction was applied to correct the acoustic modes at the Γ-point.

Electronic structures of NaTl type U*T* compounds were calculated with and without spin-polarization using scalar as well as full relativistic PAWs to account for SOC. In the latter case, the initial guess of the spin direction axis was set to the [001] direction and was kept during the optimization. We analyzed the electronic structure constructing a set of maximally-localized Wannier functions (MLWFs) from the converged ground state electronic density of the plane-wave calculations. We used the program *Wannier90* version 2.1.0 for this purpose.[36] We defined a target dimension of 36 WFs (72 WFs in case of SOC) consisting of a set of one s- and five dWFs for each d-metal atom and a set of five d- and seven f-WFs for each uranium atom. The WFs were constructed using an 8x8x8 k-points grid. We chose an energy range from the bottom of the valence band to +3.5 eV above the Fermi level E_F as frozen inner window and an outer window that included 70 bands (140 bands in case of SOC) for the disentanglement procedure. The WF basis received by this method can reproduce the plane-wave electronic structure until about +4 eV above E_F as shown in Figure S2 for the case of hp-UCo. We used the WF basis to calculate Wannier-interpolated band structures as well as densities of states (DOS) and Fermi surface planes with a fine k-points sampling of 40x40x40 and 500x500, respectively. The spin-polarization at the Fermi level $P(E_F)$ and the DOS at the Fermi level $N°(E_F)$ were derived by interpolating the DOS around E_F using a 80x80x80 k-points mesh and an integration grid of 0.1 meV. The Stoner exchange integral of the uranium atoms I_{U5f} was estimated by the averaged difference of the spin-up and spin-down on-site Hamiltonian matrix elements of Wannier-projected uranium 5f orbitals derived from spin-polarized calculations.

Crystal Orbital Hamilton Population (COHP) analysis was performed with the program *Lobster* version 2.2.1.[37–40] For this purpose, the converged ground state electronic densities of the plane-wave calculations were projected onto a set of localized orbitals. For the d-metal atoms Fe, Co, and Ni, we chose 3d and 4s orbitals, for the uranium atom 5f, 6d, as well as 6s and 6p orbitals to account for the semi-core states of the pseudopotential. These projections resulted in an absolute charge spilling of less than 3%.

Crystal structure prediction was performed with the evolutionary algorithm USPEX version 9.4.4.[22–24] USPEX only needs the composition and the number of formula units as input variables. We chose eight formula units of UCo and a population size of twenty crystal structures for each generation. The initial population was generated with random crystal structures. Each subsequent generation was generated applying the variation operators heredity (50 %), random (20 %), permutation (10 %), lattice mutation (10 %) and softmutation (10 %) as provided by the USPEX program. The trial structures from USPEX have been fully relaxed within DFT theory applying three steps of optimization with a 55 to 70 Ry kinetic-energy, a 540 to 600 Ry charge-density cutoff and a reciprocal cell resolution of 0.08 to 0.05 2π/Å. The two minimum structures of the UCo type and the NaTl type were found within 10 generations.

3. Results

3.1 Methodology

Uranium metal and uranium containing alloys that either have a substantial 5f−5f orbital overlap or a significant hybridization with bands of the alloy partner, generally display only weak correlation effects.[3] Therefore, many electronic properties of these compounds can be sufficiently described using density functional theory with the local density approximation (LDA) or generalized gradient approximation (GGA).[3,41–44] For example, Figure 1a,b displays the calculated density of state (DOS) of α-uranium with experimental lattice constants using LDA and GGA in comparison to experimental photoelectronic data of *Baer* and coworkers.[45] The spectral features *A, B,* and *C* are well reproduced by the theory. Interestingly, the calculated LDA DOS is virtually identical to the GGA DOS. *Athanasios* and coworkers calculated the band structure of α-uranium with many-body electronic structure theory finding only moderate f-electron correlation effects that are predominant in the unoccupied states.[46] Because of the low occupation of f orbitals these correlations do not strongly affect the ground state properties of uranium. In our study, we are mainly interested in predicting the properties of a possible NaTl type high-pressure phase of UCo with U−U distances of about 2.7 Å that are well below the Hill-limit of 3.4 Å[47] and are even smaller than in α-uranium (≈3.1 Å).[5] We therefore expect a pronounced

5f−5f orbital overlap and only weak correlation effects in the 5f bands that should be sufficiently described by LDA or GGA calculations.

More accurate results, especially for description of magnetism, could be achieved using DFT+DMFT (Dynamic Mean Field Theory) that accounts for dynamic effects such as spin fluctuations or band narrowing due to mass renormalization which are important effects for weakly correlated metals and alloys.[48,49] However, as DFT+DMFT is significantly more computationally demanding than standard DFT methods, its static limit, the DFT+*U* approach[50] is often used to improve the description of magnetism in uranium intermetallics, especially if it stems from localized f-electrons.[51–54]

The main effect of all DFT+*U* functionals is to shift unoccupied bands up and occupied bands down in energy.[48,50] We demonstrate this effect in Figure 1c-d, where we apply the DFT+*U* correction to the uranium 5f orbitals. Increasing the value of the Coulomb interaction *U* results in the opening of a gap at about 1.2 eV that is not present in the experimentally obtained data. It is still under debate, if the use of DFT+*U* is reliable for weakly or moderately correlated metallic systems as the incorporation of exact exchange in the subset of localized orbitals can induce unphysical effects. These may be an enhancement of the Stoner parameter, a band broadening, or a reduction of the density of states at the Fermi level.[48] These effects are even more pronounced using hybrid functionals for metallic systems as the incorporation of the exact exchange is applied to all states in the system.[55] Therefore, hybrids do not permit an improved description of the fundamental properties of metals.[55] Moreover, *Janthon* and coworkers demonstrated that hybrids neither improve the energetics nor the elastic properties of transition metals compared to PBE-GGA.[56]

Therefore, we will focus our calculations on the PBE-GGA functional. Additionally, we will include results calculated with LDA. This allows us to follow an approach proposed by *Grabowski* and coworkers who use LDA and GGA calculations as *ab initio* error bars for thermodynamic properties of fcc metals.[57] The experimental data for those elements should lie between the results of these two functionals. Examples are the general underestimation (LDA) or overestimation (GGA) of lattice parameters and the overestimation (LDA) or underestimation (GGA) of bulk moduli.[58] Moreover, we will apply LDA+*U* calculations as a "grain of salt" as suggested by *Petukhov* and coworkers to investigate the effects of static correlation.[48] We will use the rotationally invariant scheme of *Liechtenstein* and coworkers with the fully localized limit (FFL) double counting correction as implemented in *Quantum Espresso*. For most of our calculations, we will apply an effective Coulomb and exchange interaction of $U = 1.5$ eV and $J = 0.5$ eV for the uranium 5f orbitals, respectively. These values are somewhat lower than the ones obtained for uranium atoms[51,59] and are of similar magnitude as in other works investigating intermetallic uranium compounds.[51–54] In Section 3.4.2 we will investigate the effect of the magnitude of the Coulomb interaction on the electronic and magnetic properties in more detail.

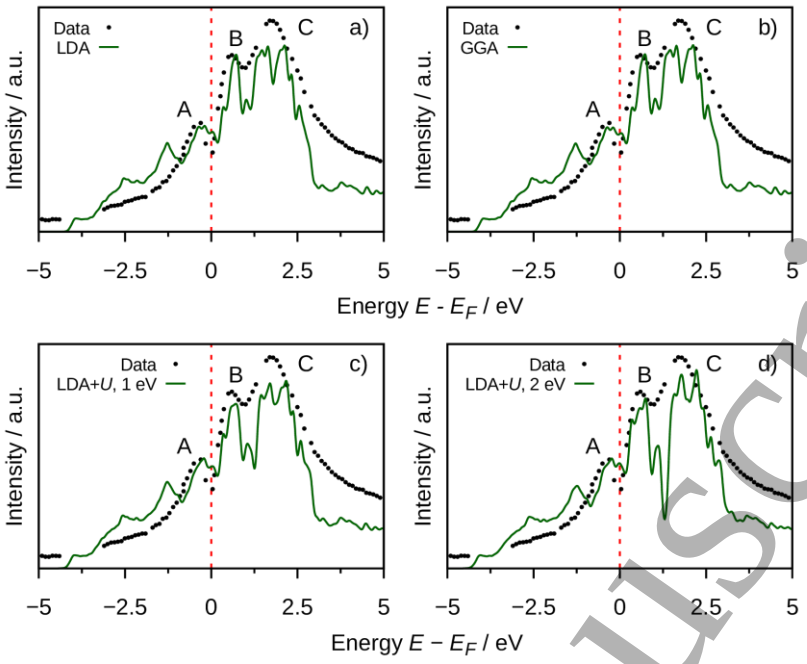

Figure 2: Calculated density of states of α-uranium (DFT/PAW+SOC) with experimental lattice constants (see Table 1) in comparison to room temperature experimental XPS and BIS spectra of Baer and coworkers[45] Spectral features are marked with letters (see text). **a)** LDA, **b)** GGA, **c)** LDA+*U* (*U* = 1 eV, *J* = 0.5 eV) and **d)** LDA+*U* (*U* = 2 eV, *J* = 0.5 eV).

3.2. Preliminary investigations

Table 1 collects crystallographic information, calculated lattice parameters, bulk moduli and heats of formation at 0 K of uranium-cobalt alloys in comparison to experimental data. The calculated lattice parameters and bulk moduli are in fair agreement with the experiments. The GGA results (Mean averaged percentage error (MAPE): lattice parameters 0.6%, bulk moduli 17%) are closer to the experimental values compared to the LDA results (MAPE lattice parameters 2.5%, bulk moduli 36%). As LDA typically "overbinds",[58] lattice parameters calculated with this method are always smaller and bulk moduli always larger than GGA results. Our LDA+*U* results are somewhat in between LDA and GGA. In case of the fcc intermetallic compound UCo_2 we find the experimental data lie between the results of LDA and GGA as suspected by *Grabowski* and coworkers[57] demonstrating the capability of these functionals as *ab initio* error bars for thermodynamic properties of fcc metals.

Table 1: Space groups (SG), Pearson symbol, lattice parameters, bulk moduli B_0 and heats of formation per atom ΔH_f of calculated UCo_x alloys using LDA, GGA and LDA+U (U = 1.5 eV, J = 0.5 eV) (PAW+SOC) in comparison to experiment. The experimental data given was collected at room temperature. DFT based ΔH_f are calculated at $T = 0$ K and $p = 0$ GPa and are compared to the $T = 0$ K values derived from the Miedema model.[60]

		SG, Pearson symbol	Lattice parameters / Å			B_0 / GPa	ΔH_f / kJ mol^{-1}	
			a	*b*	*c*		DFT	Miedema[60]
hcp Co	LDA	$P6_3/mmc, hP2$	2.434		3.886	268	–	–
	LDA+*U*		2.434		3.886	268	–	–
	GGA		2.497	–	4.038	215	–	–
	Exp[61,62]		2.5089(8)	–	4.0696(8)	199(6)	–	
UCo_2	LDA	$Fd\bar{3}m, cF24$	6.840			230	−33	
	LDA+*U*		6.870			218	−36	−31
	GGA		7.004	–	–	188	−30	
	Exp[63]		6.9924(4)	–	–	217	–	
UCo (UCo type)	LDA	$I2_13, cI16$	6.265			222	−33	
	LDA+*U*		6.274			210	−36	−33
	GGA		6.317	–	–	188	−32	
	Exp[5]		6.3557(4)	–	–	–	–	
UCo (NaTl type)	LDA	$Fd\bar{3}m, cF16$	6.096			223	−33	
	LDA+*U*		6.141			215	−35	−33
	GGA		6.244	–	–	182	−29	
	Exp		–	–	–	–	–	
U_6Co	LDA	$I4/mcm, tI28$	10.109		5.011	161	−5	
	LDA+*U*		10.145		5.173	153	−9	−10
	GGA		10.249	–	5.190	147	−10	
	Exp[11]		10.323(4)	–	5.191(4)	–	–	
α-U	LDA	$Cmcm, oS4$	2.753	5.773	4.867	176	–	–
	LDA+*U*		2.802	5.820	4.893	148	–	–
	GGA		2.817	5.869	4.923	136	–	–
	Exp[4,64]		2.8539(1)	5.8678(1)	4.9554(1)	104(2)	–	

The calculated heats of formation per atom ΔH_f are of similar magnitude for the three DFT functionals. However, only the GGA functional finds all experimental known phases (UCo_2, UCo, U_6Co) to be stable at $T = 0$ K and $p = 0$ GPa. In case of LDA and LDA+*U*, U_6Co becomes unstable against decomposition to UCo and α-U as shown by the form of the convex hulls in the top of Figure 3. However, LDA+*U* slightly reduces the error compared to LDA. It is interesting to note that our *ab-initio* approach for calculating the heats of formation (PBE/PAW+soc) reveals values that differ not more than by 1 kJ/mol from the results of the semi-empirical Miedema model.[60] Although the absolute values of formation enthalpies predicted by the Miedema model can significantly differ from experimental values, it is able to correctly predict the alloying behavior of binary alloys with a success rate of about 95% as

demonstrated by a recent study.[65] Therefore, we expect the *relative* enthalpy differences of uranium-cobalt alloys calculated by the PBE functional to be reliable.

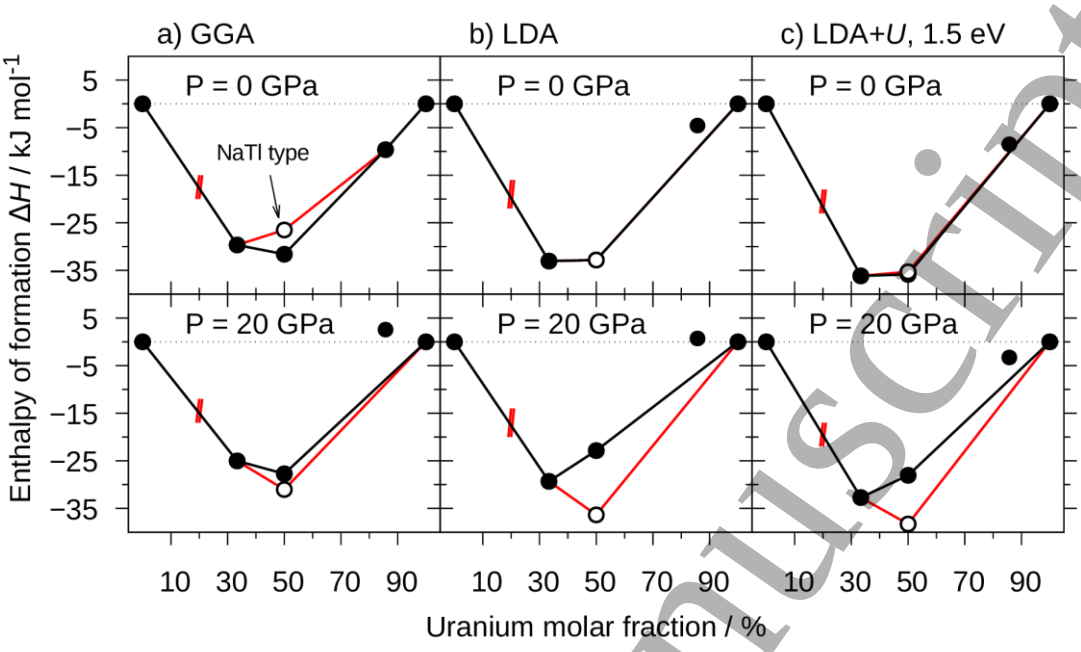

Figure 3: Enthalpies of formation per atom of the calculated UCo_x alloys at 0 GPa and 20 GPa with different functionals. (DFT/PAW+soc). **a)** LDA, **b)** GGA and **c)** LDA+*U* (*U* = 1.5 eV, *J* = 0.5 eV) Straight lines indicating the convex hull of thermodynamic stable phases (black: UCo type, red: NaTl type). The struck lines at the cobalt rich side symbolize that not all phases of the binary U-Co system are sampled. The pressure is derived from fits to the Murnaghan EOS (see Section 2 for details).

3.3. Crystal structure prediction and relative stability of hp-UCo

We performed a DFT based crystal structure prediction on the compound UCo to confirm its individual structure type. UCo crystalizes in a strongly distorted CsCl type structure as shown in Figure 1a,b.[5] Our result of the crystal structure search using the PBE functional is displayed in Figure 4a. It reveals two minimum structures: the proposed UCo type crystal structure with a unit cell volume of approximately 250 $Å^3$ and a NaTl type crystal structure with an approximate volume of 240 $Å^3$. The phonon dispersion of the NaTl type UCo at 0 GPa (Figure S3) do not exhibit any instability in form of “soft” modes with imaginary frequencies characterizing this compound as a real local energy minimum.

The analysis of the pressure dependency of the enthalpy difference of the two UCo phases is shown in Figure 4b. The variation of Δ*H* with pressure demonstrates that the NaTl type structure should be a high-pressure phase of UCo. Moreover, hp-UCo should be stable against decomposition in the adjacent phases UCo_2 and U_6Co at 0 K and elevated pressures as shown by the form of the convex hulls at the bottom of Figure 3.

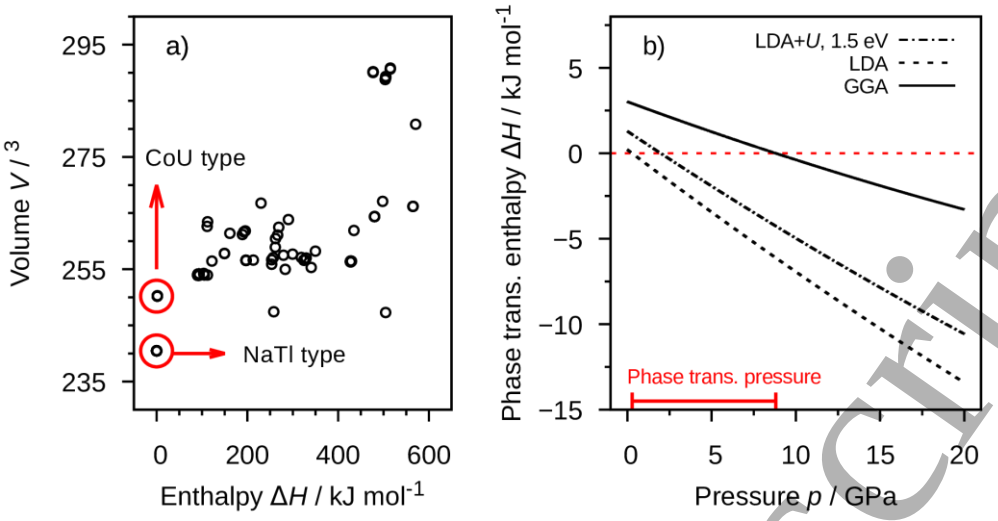

Figure 4: USPEX crystal structure prediction results and relative stability of hp-UCo. **a)** Energy/unit cell volume distribution of the sampled structures (PBE/PAW sp). **b**) Pressure dependency of the difference of the total energy per atom of the UCo type phase and the NaTl type phase calculated with different functionals (DFT/PAW sp+soc). The pressure is derived from fits to the Murnaghan EOS (see Section 2 for details).

It is reasonable to find the NaTl-type phase being a high-pressure phase as it has a smaller unit cell volume than the UCo type phase (see Table 1). Because of its larger volume, the UCo type becomes unstable at higher pressures as the *pV* term of the enthalpy Δ*H* increases faster with pressure than for the NaTl type hp-UCo. The LDA calculations predict a phase transition pressure of about 0.1 GPa, whereas GGA predicts a much higher value of about 9 GPa. The LDA+*U* results lie between these two extremes. The difference stems from the effect that LDA predicts a higher volume difference of the two phases than GGA, making *p*Δ*V* greater. As demonstrated for UCo_2 in the last section, we also want to adopt the concept of *ab initio* error bars to hp-UCo predicting that the phase transition pressure of hp-UCo lies between the LDA and GGA results as highlighted in Figure 4b.

3.4 Electronic and magnetic properties of hp-UCo

3.4.1 Magnetic ordering in hp-UCo

We find hp-UCo to order ferrimagnetically with a total spin magnetic moment of 0.92 μ_B per formula unit. The uranium spin magnetic moments (0.89 μ_B) are aligned antiparallel to the cobalt spin magnetic moments (−0.16 μ_B). As the atomic moments are approximated within atomic spheres, they do not necessary sum up to the total moment. We neglected the orbital contribution to the total magnetic moment in our calculations as these moments were not accessible with our computational approach. Whereas this is typically an appropriate simplification for the 3d metals, a significant amount

of orbital contributions of the uranium atoms to the total magnetic moment is expected.[1–3] First results using the "all-electron full-potential linearized augmented-plane wave" code *Elk*[66] yield orbital magnetic moments inside the uranium muffin-tin spheres that are of similar magnitude but aligned *antiparallel* to the uranium spin magnetic moments. Therefore, we expect the total magnetic moment of hp-UCo to be significantly reduced due to orbital magnetic contributions.

We tested different starting magnetic orientations using spin-polarized calculations without spin-orbit interactions to confirm the ferrimagnetic ground state. For that, we used the MAXMAGN-toolkit from the *Bilbao Crystallographic Server*[67,68] to construct the maximal magnetic space groups of the space group $Fd\bar{3}m$ (No. 227) of the paramagnetic phase using a single propagation vector along the crystallographic *c* axis. From the results we chose only those spin-configurations that were oriented parallel or antiparallel to the *c* axis. The spin orientations of the resulting four different starting magnetizations are available from Figure S4. In cases, where the uranium magnetic moments were aligned antiparallel to each other, the calculations always converged into the non-magnetic solution that is about 6 mRy higher in energy than the ferrimagnetic solution. In cases with uranium spin moments aligned in parallel, always the ferrimagnetic solution was obtained. We thus conclude that the ferrimagnetic solution with the uranium magnetic moments aligned antiparallel to the cobalt magnetic moments is the magnetic ground state of hp-UCo.

The U–U distances in hp-UCo are about 2.7 Å and thereby well below the Hill-limit of 3.4 Å for the onset of localized magnetism[47]. Therefore, we should characterize hp-UCo as an itinerant magnet. The average U–U near-neighbor distance of the nonmagnetic room-pressure phase of UCo is 3.2 Å.[5] The onset of magnetism in the high-pressure phase is therefore quite counterintuitive as it results from a *compression* of the U-U distance.

The ferrimagnetic ordering of hp-UCo can be understood applying the concept of covalent magnetism and the Stoner model.[69] Both models are well established for describing the itinerant magnetism of metals and alloys and should therefore be valid for our system.[69] The Stoner model states that the gain in exchange energy by a rigid-band shift of the spin-up and spin-down band stabilizes a ferromagnetic ground state, if the Stoner criterion (Eq. 2)

$$I \cdot N°(E_F) > 1 \qquad (2)$$

holds, whereas *I* is the Stoner exchange integral and $N°(E_F)$ is the density of states (DOS) per atom and spin at the Fermi energy of the non-magnetic state.

Figure 5a displays the DOS of non-magnetic hp-UCo. It consists of a well separated band located approximately 4 eV below E_F, followed by a cobalt 3d valence band ranging from −3.5 eV to −0.5 eV and an uranium 5f conduction band that is predominantly located above E_F with a band width of approximately 3 eV. This band order is in line with the electronegativity difference of the elements. The valence band and conduction band are separated by a gap of approximate $\Delta_{3d,5f} = 0.1$ eV. The

Fermi level lies in a pronounced maximum of the DOS in the conduction band. We calculated the Stoner exchange integral of the uranium atoms I_{U5f} and $N°(E_F)$ to 0.59 eV and 2.66 eV^{-1}, respectively. Thus, the Stoner criterion holds for hp-UCo.

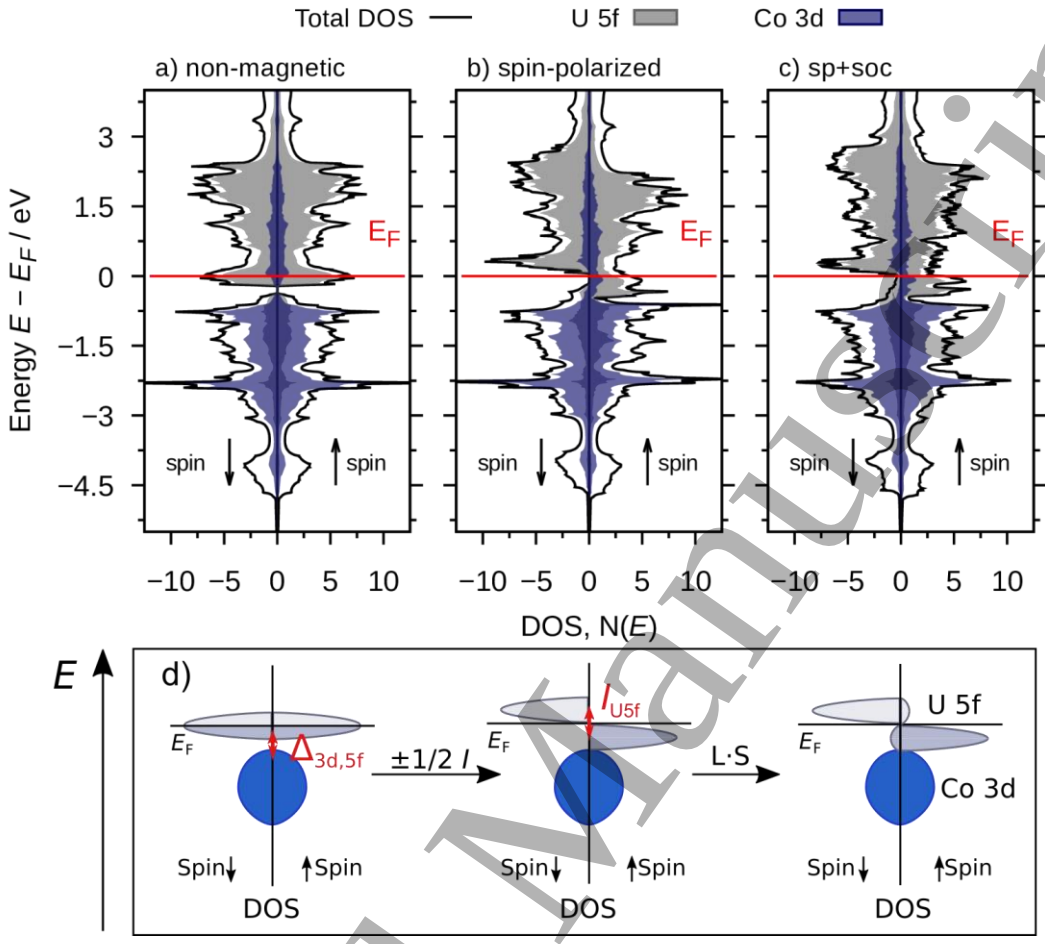

Figure 5: a)-c) Spin-projected DOS and pDOS of hp-CoU. Overlap of U 5f and Co 3d pDOS are highlighted with a filling with darker color. **a)** PBE/PAW non-magnetic **b)** PBE/PAW spin-polarized **c)** PBE/PAW spin-polarized + SOC; The spin quantization axis is set to the [001] direction. **d)** Sketch of the DOS highlighting quantities used in the following text: the band gap $\Delta_{3d,5f}$ between the Co 3d valence and U 5f conduction band and the Stoner exchange integral I_{5f} of the uranium atoms.

Indeed, the spin-resolved uranium 5f pDOS of the magnetic ground state can be well approximated by a rigid-band shift of the uranium 5f pDOS of the non-magnetic solution as shown in Figure 5a and b. As a result, the overlap of the uranium 5f spin-up states with the corresponding cobalt 3d-states increases. The hybridization of these two bands shift some spectral weight of the cobalt 3d spin-up states above the Fermi level. In case of the spin-down states, the hybridization is suppressed as the gap between 5f conduction and 3d valence band increases and the spectral weight is not redistributed. In sum, this results in a magnetic polarization of the cobalt atoms antiparallel to the uranium atoms and to the ferrimagnetic ground state. The effect of hybridization induced magnetization is discussed

under the term covalent magnetization[69,70] and is used to explain the occurrence of ferrimagnetic intermetallic compounds such as $ZrFe_2$.[71] As we will discuss in Section 3.4.3, the effect of covalent magnetization in NaTl type U*T* compounds (*T*: Fe, Co, Ni) increases by reducing the band gap $\Delta_{3d,5f}$, so that in case of UFe this effect becomes the dominant contribution to the magnetization.

The spin-splitting of the uranium 5f conduction band shifts all spin-down states above the Fermi level, separating it by a band gap of approximately 0.3 eV from the cobalt 3d valence band (Figure 5b). This makes the spin-down channel semiconducting, whereas the spin-up channel remains metallic. Consequently, the DOS at E_F is fully spin-polarized. This characterizes hp-UCo as a half-metallic ferrimagnet. A half-metal is defined to have a spin-polarization of $P(E_F) = 100\,\%$ at the Fermi level.[17,18] This definition is a hypothetical situation that holds only in the limit of vanishing temperature and neglecting spin-orbit interactions.[18] Therefore, it is some kind of "common sense" that the strong spin-orbit interactions of heavy elements destroy half-metallicity. Neglecting spin-orbit interactions, hp-UCo possess 100 % spin-polarization at E_F as stated above. However, we expect the heavy-atom uranium to show strong spin-orbit coupling effects. Surprisingly, a calculation including spin-orbit interactions (Figure 5c) reveals that the overall shape of the DOS remains preserved for the most part. Moreover, the spin-polarization at E_F is only reduced to about 90 %. Figure 5d sketches this effect and summarizes the discussion above.

3.4.2. Influence of the DFT functional on the electronic and magnetic properties

We investigated the influence of different DFT functionals on the magnetic and electronic properties of hp-UCo to get a deeper understanding which factors promote a high spin-polarization at the Fermi level. For that, we compared the results of the GGA calculations with those of LDA and LDA+*U* as outlined in Section 3.1.

The results are summarized in Table 2. The calculated DOS's are compared in Figure S5. The magnetic moments calculated by LDA are about 50 % smaller compared to the GGA results. Both functionals yield similar values for DOS $N°(E_F)$ and the band gap $\Delta_{3d,5f}$ of the non-magnetic calculations. The most significant difference between these two functionals is that LDA yields virtually no spin-polarization at E_F. The reason is the reduced exchange splitting of the 5f band compared to the GGA results. Due to the smaller Stoner exchange integral I_{U5f} the spin-up states of the uranium 5f orbitals are not lifted above E_F as in case of the GGA calculations resulting in no spin-polarization at E_F. LDA+*U* increases the exchange interactions giving similar results as the GGA functional.

The effect of the different functionals on the spin-polarization at E_F is nicely visible comparing the spin-polarized Fermi surfaces. Figure 6 displays a representative cross section of the Fermi surface of hp-UCo. The GGA and LDA+*U* cross sections in Figure 6a,c are dominated by the contribution of the majority-spin channel. Most of the *minority*-spin density is found along the Γ-X path of the Brillouin zone. The Fermi surface of the LDA calculation (Figure 6b) contains a significant amount of both spin densities resulting in a spin-polarization of approximately 50 %.

Table 2: Calculated magnetic and electronic properties of hp-UCo using different functionals. Total spin moment μ_{tot}, atomic spin moments μ_U and μ_{Co}, non-magnetic DOS at E_F $N°(E_F)$, Stoner exchange integral I_{U5f} of the uranium atoms, band gap $\Delta_{3d,5f}$, spin-polarization at the Fermi level $P(E_F)$ (see Section 2 for details of the calculations). The equilibrium lattice parameters *a* used for the calculations are also given.

	GGA	LDA	LDA+*U*
μ_{tot} / μ_B	0.92	0.42	0.95
μ_U / μ_B	0.89	0.37	0.89
μ_{Co} / μ_B	−0.16	−0.03	−0.12
$N°(E_F)$ / eV^{-1}	2.66	2.03	2.17
I_{U5f} / eV	0.59	0.38	0.70
$\Delta_{3d,5f}$ / eV	0.12	0.11	0.10
$P(E_F)$	0.91	0.53	0.85
a / Å	6.244	6.096	6.141

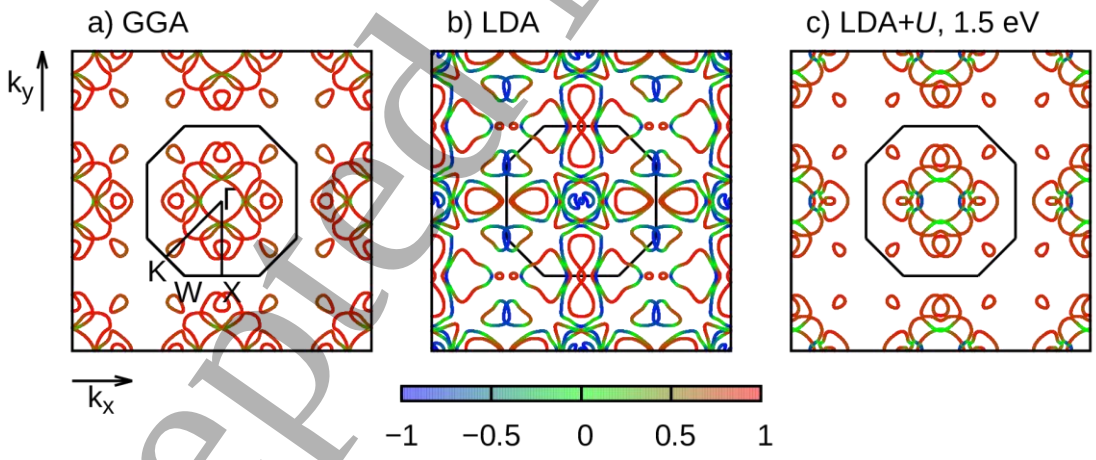

Figure 6: Spin-projected Fermi surface cross sections cut by the [110]-[011] plane at $k_z = 0$ of hp-CoU calculated with different functionals (DFT/PAW, sp+soc, spin quantization axis along [001]). **a)** GGA **b)** LDA and **c)** LDA+*U* (*U* = 1.5 eV, *J* = 0.5 eV). Red: 100 % spin↑, Blue: 100 % spin↓. The border of the first Brillouin zone is shown as a black line. High-symmetry points are labeled.

As shown in Table 2, the three tested functionals yield quite different equilibrium lattice parameters *a*. To estimate the effect of the lattice parameter on the electronic and magnetic properties of hp-CoU, we performed calculations at different values of *a*. This also provides information about the pressure dependency of these properties. The results are summarized in Figure 7. As discussed in section 3.2., the experimental lattice parameters should lie between the calculated GGA and LDA equilibrium values. This corresponds to the shaded regions in Figure 7.

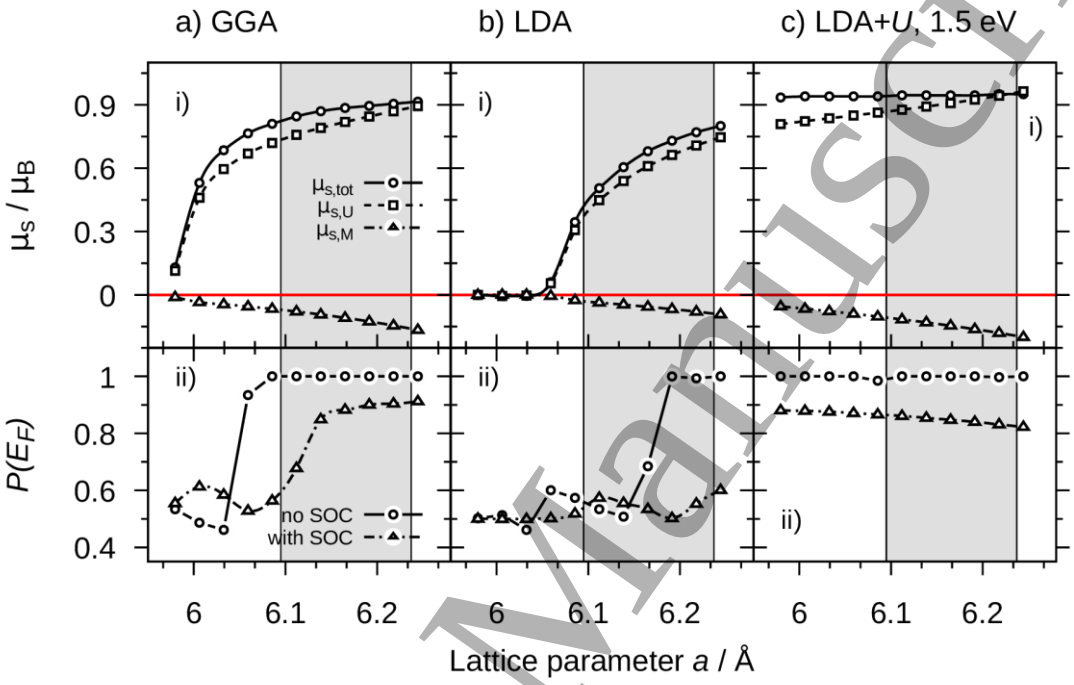

Figure 7: Dependency of selected magnetic and electronic properties on the size of the lattice parameter *a* calculated with different functionals: **a)** GGA **b)** LDA, and **c)** LDA+*U* (*U*=1.5 eV, *J*=0.5 eV). **i)** Total and atomic spin magnetic moment μ_s per primitive unit cell (DFT/PAW sp+soc, spin axis along [001]). **ii)** Spin-polarization at the Fermi level $P(E_F)$ (LDA+*U*/PAW sp and LDA+*U* /PAW sp+soc). The lines are guide for the eyes. The shaded region marks the ab initio error bars. The experimental lattice parameter should lie in this region. See Section 2 for computational details.

The spin magnetization decreases by lowering *a* in case of GGA and LDA calculations (Figure 7a-i,b-i). The LDA calculations yield a non-magnetic ground state below a lattice parameter of 6.05 Å. The suppression of magnetization by pressure or equivalently by reducing *a* is in line with characterizing hp-CoU as an itinerant magnet.[2] This behavior was already proposed before because of the small U–U atomic distances in hp-UCo that are well below the Hill-limit.[47]

The total spin moment of the LDA+*U* calculations stays constant over the whole investigated lattice parameter range. This illustrates the effect of the LDA+*U* correction to push the system into localized electronic states. The independency of the magnetic moment on pressure is a known behavior of well-

localized electrons as observed for example for the 4f electrons of the lanthanoids.[69] Thus, it could be doubtful, if the applied LDA+*U* correction is valid for our system as it does not catch the expected itinerant behavior of the 5f electrons.

As does the magnetization, also the spin-polarization $P(E_F)$ (Figure 7c-iii), stays constant in case of the LDA+*U* calculations. The plain LDA results yield spin-polarizations of 100 % only without spin-orbit interactions and for lattice parameters exceeding 6.2 Å. Including spin-orbit coupling $P(E_F)$ vanishes to its unpolarized limit of 50 % for the entire lattice parameter range investigated. In case of PBE calculations, including spin-orbit interactions the spin-polarization remains above 90 % up to a lattice parameter of approximately 6.15 Å. For lower values of the lattice parameter *a* it reduces successively to 50 %. Decreasing the lattice parameter induces a shift of the minority-spin bands across the Fermi level which increases $N(E_F)$ as well as reduces $P(E_F)$.

We further investigated the effect of the effective Coulomb parameter *U* of the LDA+*U* calculations on the electronic structure of hp-UCo. The results are collected in Figure 8. As we fixed the value of the effective exchange parameter to $J = 0.5$ eV for all calculations, the results for $U = 0$ eV do not correspond to the plain LDA calculation.

Increasing the effective Coulomb parameter *U* has two main effects: First, it reduces the band gap $\Delta_{3d,5f}$ between the uranium 5f conduction and the cobalt 3d valence band (Figure 8d) as LDA+*U* typically shifts occupied bands to lower energies.[50] Second, the value of the Stoner exchange integral I_{U5f} of the uranium atoms (Figure 8e) increases with increasing *U*. This is also expected from the LDA+*U* correction. For the applied fully localized limit (FLL) double counting correction, *I* should follow the expression (Eq. 3)

$$I_{FLL} \approx (U + 2 \cdot l \cdot J)/(2 \cdot l + 1) \quad (3)$$

whereas l is the angular momentum quantum number of the orbitals used for the LDA+*U* correction (here: $l = 3$).[48] This is found for *U* values between 0.5 eV and 2 eV (see Figure 8e).

For a magnetic ground state, a certain value of the Stoner exchange integral is needed to fulfill the Stoner criterion (Equation 2). For $U = 0$ eV the Stoner criterion is not satisfied resulting in a non-magnetic ground state. (Figure 8a) With increasing *U* the total spin magnetic moment increases until $U = 2$ eV. For higher values of *U* it stays nearly constant. The main contribution to the total spin moment stems from the uranium atoms. With increasing *U* the spin-polarization of the cobalt atoms increases significantly. This is mainly due to a reduction of the band gap $\Delta_{3d,5f}$ between the conduction and valence band (Figure 8d). As discussed in the previous section, an increase of the overlap of the uranium 5f and cobalt 3d-states results in a magnetic polarization of the cobalt atoms antiparallel to the moments of the uranium atoms in the spirit of the concept of covalent magnetization.[69]

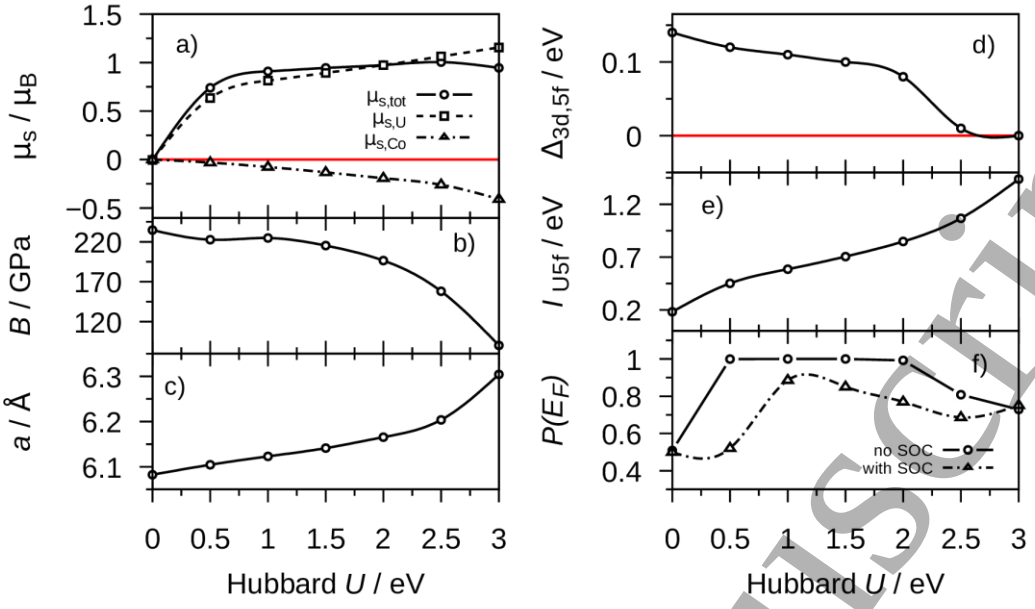

Figure 8: Dependency of selected magnetic, electronic, and structural properties on the choice of the effective Coulomb parameter *U*. The value of the exchange parameter was fixed to *J* = 0.5 eV for all calculations **a)** Total and atomic spin magnetic moment μ_s per primitive unit cell. (LDA+*U*/PAW sp+soc, spin axis along [001]) **b)** Bulk moduli *B* and **c)** equilibrium lattice parameter *a* derived from the Murnaghan equation of state (LDA+*U*/PAW sp+soc), **d)** Band gap $\Delta_{3d,5f}$ between the M_{3d} valence and U_{5f} conduction band (LDA+*U*/PAW), **e)** Stoner exchange integral I_{U5f} of the uranium atoms (LDA+*U*/PAW sp), **f)** Spin-polarization at the Fermi level $P(E_F)$ (LDA+*U*/PAW sp and LDA+*U* /PAW sp+soc). The lines are guide for the eyes. See Section 2 for computational details.

A half-metallic ground state with 100 % spin-polarization is calculated for *U* values between 0.5 eV and 2 eV for calculations without spin-orbit coupling (Figure 8f). For $U < 0.5$ eV a too small Stoner exchange parameter prohibits the shift of the 5f minority-spin states above the Fermi level resulting in no spin-polarization at E_F. For $U > 2$ eV, it is the increased overlap of the uranium 5f states with the cobalt 3d-states due to the vanishing band gap $\Delta_{3d,5f}$ that reduces $P(E_F)$. Including spin-orbit coupling, there is only a small range of *U* values around 1 eV that lead to a spin-polarization over 90 %. For smaller *U* values, the marginal energy difference between the two spin channels enables an effective mixing by the spin-orbit interactions resulting in no spin-polarization at E_F. For $U > 1$ eV, the spin-polarization at E_F decreases nearly linearly with increasing *U*. This behavior could result from exchange enhanced spin-orbit coupling effects that *Bultmark* and coworkers discuss for various metallic actinoid compounds.[72] By applying a multipole decomposition of the LDA+*U* energy they report that the inclusion of the Hartree-Fock exchange interaction by the Hubbard correction increases the spin-orbit coupling effects. Work is in progress to apply this method to hp-CoU.

As discussed above, it is a subtle interplay of three parameters – the band gap $\Delta_{3d,5f}$, the Stoner exchange integral I_{U5f} of the uranium atoms, and the magnitude of spin-orbit interactions – that can lead to a high amount of spin-polarization at E_F and thus to the occurrence of half-metallic properties in hp-UCo. Moreover, we suggest that it is the symmetry of the crystal structure that promotes this kind of properties. This assumption is supported by the fact that the NaTl crystal structure type is closely related to the MgAgAs structure type[21] that includes the first reported half-metallic ferromagnet NiMnSb.[17] However, for any functional used, the inclusion of spin-orbit interactions do not preserve the 100 % spin-polarization. Thus, strictly speaking, hp-UCo is no half-metal. From the view of the PBE functional, our calculations should reveal only the lower limit of spin-polarization, as it is known to drastically underestimate band gaps of semiconductors and of half-metals.[73,74] We expect from sophisticated methods, for example DFT+DMFT, that they should account better for electron correlation effects of the uranium 5f electrons[48], to increase the band gap of the minority-spin channel and therefore the spin-polarization at the Fermi level. However, as demonstrated by the LDA+*U* calculations also an influence on the magnitude of the spin-orbit interactions should be expected that makes a prediction of the actual occurrence of half-metallicity in hp-UCo problematic. Nevertheless, we demonstrate with hp-UCo that also materials with *heavy* elements can be interesting candidates for half-metallicity as suggested by *Picket* and *Eschrig*.[19]

3.4.3. Influence of the valence electron concentration on the electronic and magnetic properties

We investigated the effect of the valence electron concentration (VEC) on the electronic and magnetic properties for the compounds U*T* (*T*: Fe, Co, Ni) and alloys of them, by performing GGA, LDA, and LDA+*U* calculations. The mixed occupations at the transition metal sites were calculated in the spirit of the virtual crystal approximation (VCA) by constructing pseudopotentials with odd valence. Details concerning the calculations can be found in Section 2. The results are given in Figure 9.

The three investigated functionals yield similar dependencies of the lattice parameter *a*, the band gap $\Delta_{3d,5f}$ and the spin magnetic moments on the VEC. The lattice parameter *a* (Figure 9-v) runs through a minimum at a VEC between 7.2 and 7.5 indicating that the most stable phases should be obtainable here. The band gap $\Delta_{3d,5f}$ (Figure 9-ii) increases successively with increasing VEC running through a maximum at a VEC of 8. This is induced by a shift of the 3d valence band to lower energies with increasing atomic number of the d-metal. Increasing $\Delta_{3d,5f}$ reduces the 3d/5f band overlap and the contribution of the 3d-states to the states at the Fermi level. This is apparent comparing the non-magnetic DOS's of UFe, UCo and UNi displayed in Figure 10a,d,g. This effect is well known for uranium

intermetallics and is discussed in detail for the binary alloys crystalizing in the Au_3Cu crystal structure type.[2,3]

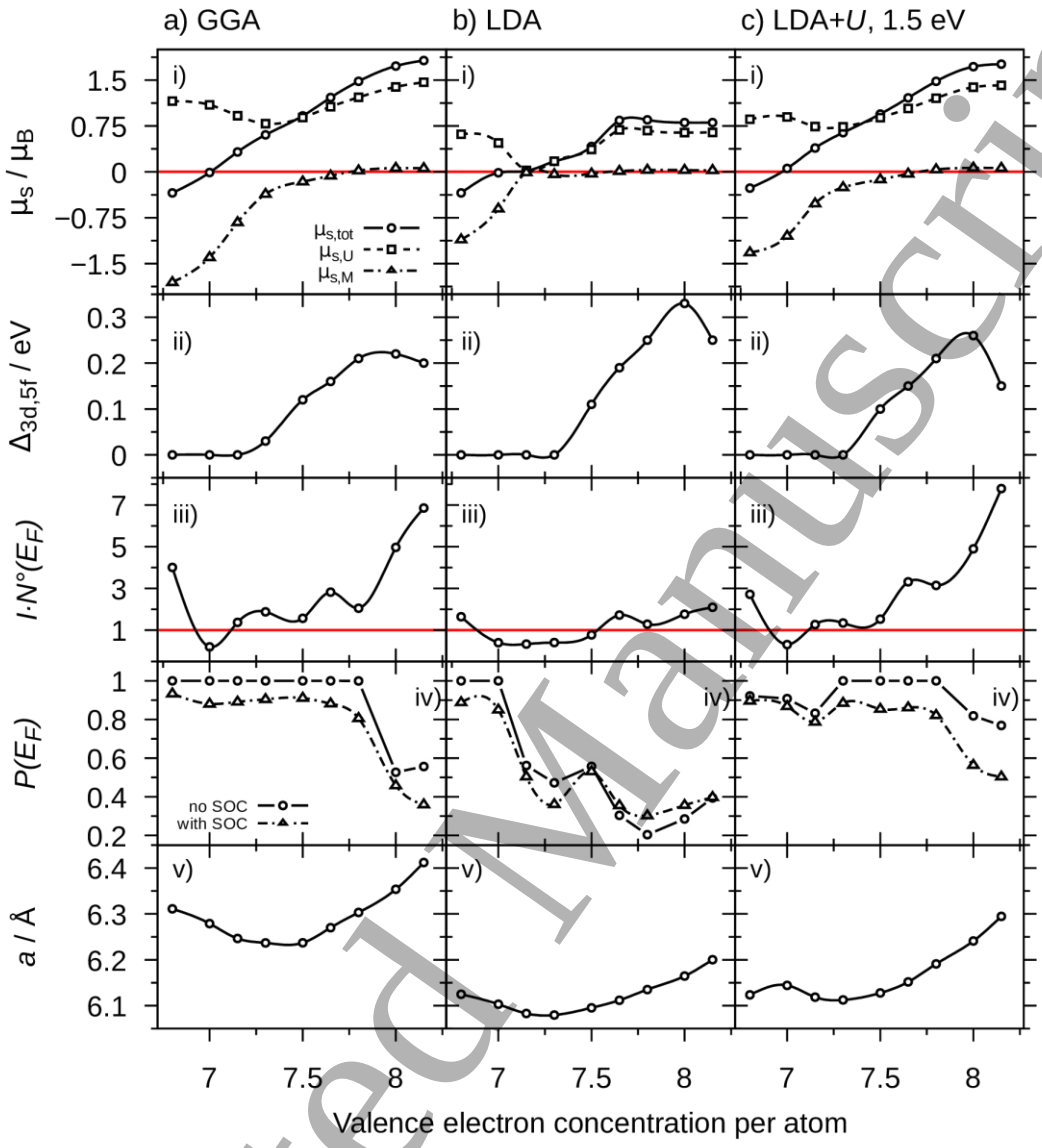

Figure 9: Dependency of selected magnetic, electronic and structural properties on the valence electron concentration per atom (VEC) of hp-U*T* applying the functionals **a)** LDA, **b)** GGA and **c)** LDA+*U* (*U* = 1.5 eV, *J* = 0.5 eV). A VEC of 7, 7.5, and 8 corresponds to the compounds UFe, UCo, and UNi, respectively. Mixed occupancies at the transition metal sides were modeled via the virtual crystal approximation (VCA). **i)** Total and atomic spin magnetic moment μ_s per primitive unit cell (DFT/PAW sp+soc, spin axis along [001]). **ii)** Band gap $\Delta_{3d,5f}$ between the M_{3d} valence and U_{5f} conduction band (DFT/PAW). **iii)** Product of the non-magnetic DOS at E_F $N°(E_F)$ and the Stoner exchange integral I_{U5f} of the uranium atoms, **iv)** the spin-polarization at the Fermi level $P(E_F)$ (DFT/PAW sp and DFT/PAW sp+soc, spin axis along [001]), **v)** the lattice parameter *a* from structural optimization (DFT/PAW sp). The lines are guide for the eyes. See Section 2 for computational details.

At a VEC > 7.5 the total spin moment (Figure 9-i) is dominated by the contributions of the uranium atoms and can be explained in terms of the Stoner model by a rigid-band shift of the uranium 5f orbitals.[69] The small spin moment of the transition metal atoms that is aligned in parallel to the spin moments of the uranium atoms results from a rudimentary hybridization between the transition metal 3d and uranium 5f band as illustrated for UNi in Figure10 h. For a VEC < 7.5 a spin moment on the transition metal sites arises that is aligned antiparallel to the spin moments of the uranium atoms. With decreasing VEC the magnitude of the transition metal atomic spin moment increases as the 3d band is successively emptied and the band gap $\Delta_{3d,5f}$ vanishes.

The ferrimagnetic ordering in this VEC region cannot be explained in terms of the Stoner model anymore. This is especially obvious for the compound UFe as all three functionals find the Stoner criterion not fulfilled for it (Figure 10-iii). For UFe the spectral weight of the spin-up band is strongly redistributed (Figure 10-b). Thus, the magnetism of UFe cannot be explained by a rigid-band shift as in case of UNi, where the spin-up and spin-down bands retain virtually the same shape in the spin-polarized state (Figure 10-h). The magnetism in the compound UFe stems from hybridization effects of the iron 3d and uranium 5f-states that can be interpreted by the concept of covalent magnetism.[69,70] In the spin-polarized DOS (Figure 10-b) of UFe the hybridization is strongly enhanced in the “spin-up” channel compared to the non-magnetic DOS (Figure 10-a). Only for this spin channel the hybridization of the bands shifts the iron 3d-states above and the uranium 5f-states below E_F, resulting in a ferrimagnetic ordering of the magnetic moments. It is interesting to note, that UFe is unique compared to the other investigated compounds as at this VEC the total spin moment is zero (Figure 9-i).

In case of the GGA and the LDA+*U* functional the spin-polarization at E_F remains over 80 % between a VEC of 6.8 and 7.7. For a VEC ≤ 8 also the LDA functional yields high values of $P(E_F)$ and even higher values of $P(E_F)$ as LDA+*U*. As discussed above, the magnetization and the half-metallic properties of UFe stems from hybridization effects. LDA captures these effects well due to its property of “overbinding”. In case of hp-UCo, LDA does not result in half-metallic properties as it underestimates the value of the Stoner exchange integral compared to GGA and LDA+*U* as discussed in Section 3.4.2. LDA+*U* localizes the uranium 5f-states and thus reduces their hybridization with the iron 3d-states. This leads to a slight lower value of $P(E_F)$ compared to LDA. All three tested functionals yield high values of $P(E_F)$ for UFe. Therefore, we think this compound is an even more interesting candidate for half-metallicity than hp-UCo. Moreover, as the DOS at E_F consists of a higher amount of transition metal 3d-states than the DOS of hp-UCo, the effect of spin-orbit interactions on reducing $P(E_F)$ should be less pronounced.

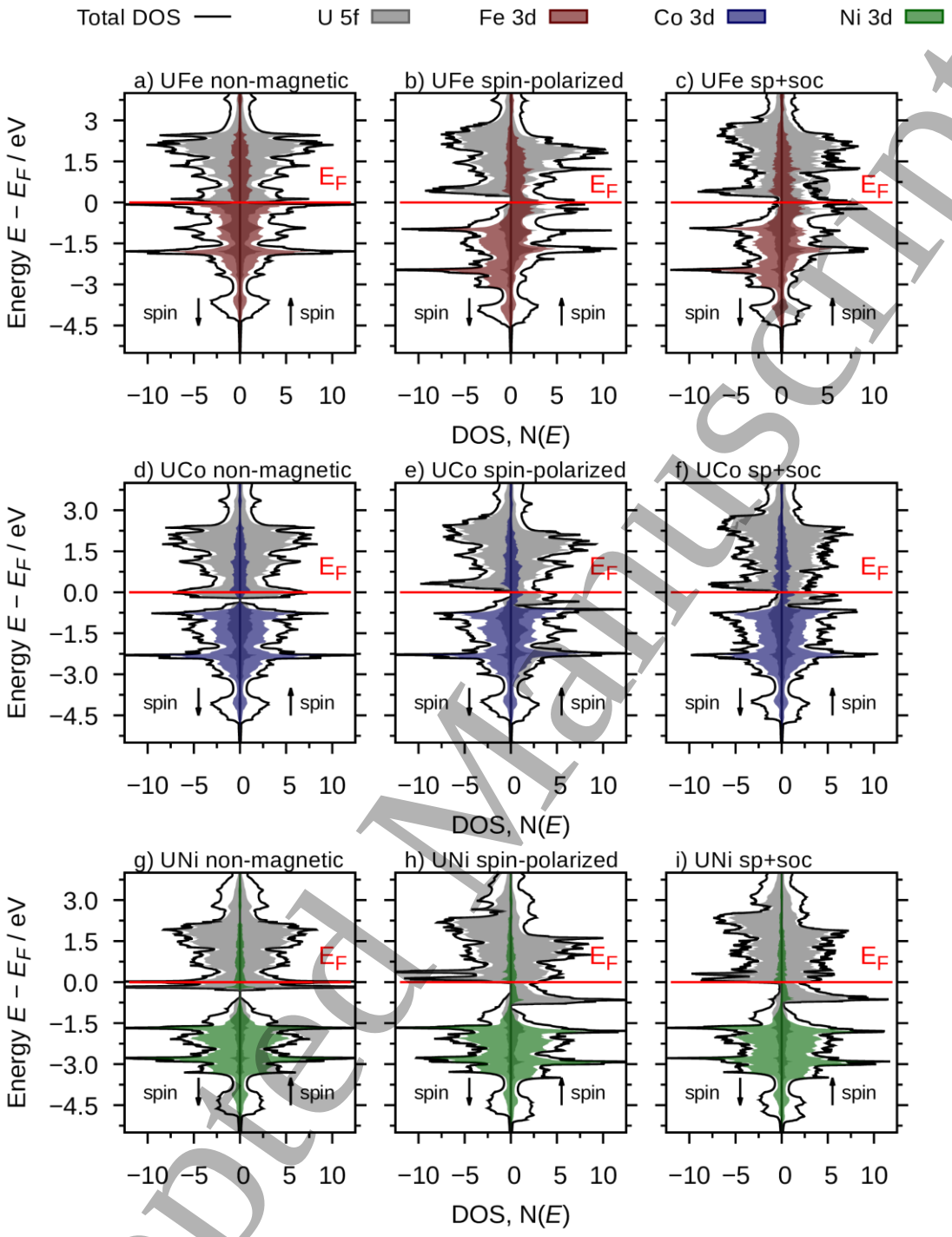

Figure 10: Spin-projected DOS and pDOS of NaTl type UFe, UCo and UNi. Overlap of U 5f and transition metal 3d pDOS are highlighted with a filling with darker color. **a), d), g):** PBE/PAW non-magnetic **b), e), h)** PBE/PAW spin-polarized **c), f), i)** PBE/PAW spin-polarized + SOC; The spin quantization axis is set to the [001] direction.

3.5 Comparison to experiments and chemical bonding in hp-UCo

In this section, we will restrict ourselves to calculations with the PBE functional. To compare our findings with the experimentally obtained data we adopt the concept of near-neighbor diagrams as introduced by *Pearson*.[21] It is useful for comparing compounds of the same crystal structure to achieve information about structure directing factors. According to *Pearson*, metal atoms *M* and *N* of a binary alloy MN_n are described by compressible spheres characterized by the atomic radii r_M and r_N. Contacts such as *M–M, M–N, N–N,* and so on, can then be formed by successively compressing these atoms. The contacts are established if the interatomic distances d_{MM}, d_{MN}, d_{NN} equal to $2r_M$, $r_M + r_N$ or $2r_N$, respectively. Plotting the radius ratio r_M/r_N against the strain parameter $(2r_M - d_{MM})/2r_N$, straight lines can be drawn representing the "strain free" contacts. Usually the *M–M* contact line is set to zero as a reference. A near-neighbor diagram is read as follows: If an alloy is located on a zero-strain *M–N* line then, according to the assumptions of the model, strain free *M–N* contacts are established in this compound. If an alloy is located below such a line these contacts are not established. If it is located above such a line the contacts are compressed.

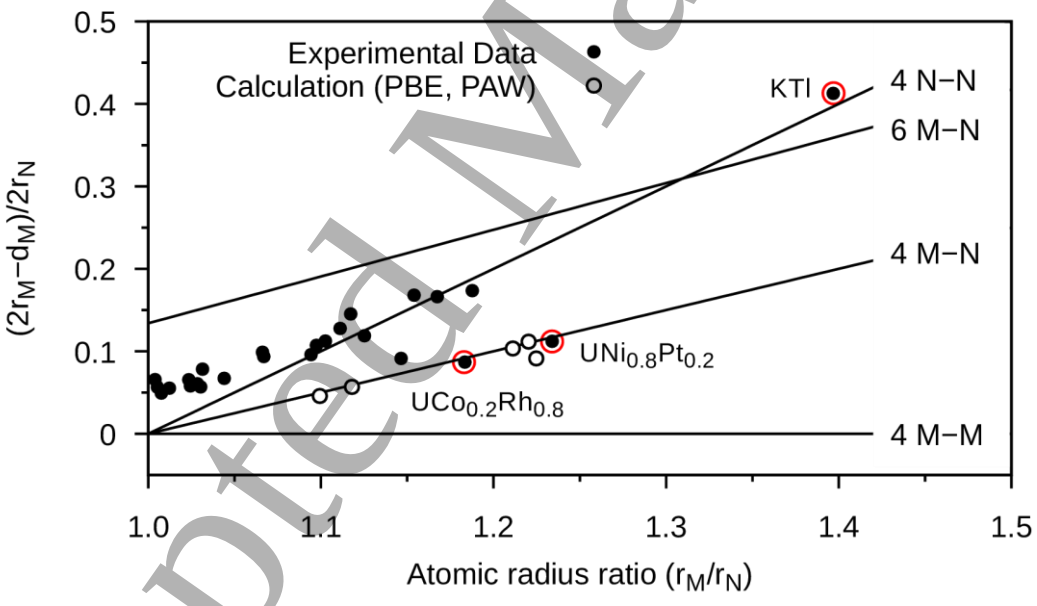

Figure 11: Near-neighbor diagram for binary and pseudo-binary phases with the NaTl (*cF16*) *MN* structure. *M* is taken as the larger of the two atoms. Numbers indicate the number of neighbors for contacts *N–N, M–N*, etc. Lines indicate strain-freeness for the labeled atomic contacts. Filled circles correspond to existing compounds. Their atomic radii were adjusted to C.N. 8. Emphasized compounds (red circles) are referred in the text. Open circles represent the calculated compounds UFe, UCo, UNi, URh, and UIr (PBE/PAW, sp). The uranium atoms are taken as the larger *M* component. The atomic radii were chosen from calculated bcc lattices of the elements (see Table S3 in the supporting information).

Figure 11 displays the near-neighbor diagram for binary and pseudo-binary alloys with the NaTl (*cF16*) *MN* structure. The experimental data was derived from *Pearson's Crystal Database*.[75] The atomic radii from *Teatum, Gschneidner,* and *Waber*[76] were adjusted from the metal atomic radii to the coordination number eight as explained by *Pearson*.[21] We calculated the crystal parameters of the compounds UFe, UCo, UNi, URh, and UIr (PBE/PAW, sp). Their atomic radii were chosen from calculated bcc lattices of these elements. The calculated crystal parameters are summarized in Table S3. As shown in Figure 11 the compounds can be classified into two groups. Most of the phases are located around the 4×*N*−*N* contact line. These are the "classical" NaTl phases formed by the group 1 alkali metals with the group 12 and group 13 metals.[21,77]

The second group consist of the pseudo-binary alloys $UCo_{0.2}Rh_{0.8}$[78] and $UNi_{0.8}Pt_{0.2}$[79] and the predicted compounds UFe, UCo, UNi, URh, and UIr derived from our calculations. They follow the 4×*M*−*N* contact line. According to *Simon* it is possible to define a "guideline" for the near-neighbor diagram of each structure type.[77] Compounds located on this line follow *Vegard's* law in such a way that their shortest interatomic distances equal the weighted sum of their atomic radii after their atomic composition. For example, a compound with the composition MN_n and the atomic radii r_M and r_N should have the following shortest interatomic distance d_0 (Eq. 4):

$$d_0 = \frac{2}{n+1}(r_M + n \cdot r_N) \quad (4)$$

In case of the NaTl structure type the guideline corresponds to the 4x *M*−*N* contact line. Phases located at this line can therefore simply be described as an ordering variant of a bcc solid solution following *Vegard's* law. As the compounds UFe, UCo, UNi, RhU, and UIr follow this guideline they should therefore be designated as ordered solid solutions.

In the NaTl structure type (*MN*) each atom *M* is equally surrounded by four *M* and four *N* atoms in the first coordination shell. The arrangement of the *M* and *N* atoms in the NaTl structure type is unusual for *MN* alloys. Generally, the nearest neighbors of an atom are of the same kind to maximize the number of hetero-atomic contacts.[80] For example, this type of ordering is adopted in the CsCl structure type (see Figure 1). According to *Pearson*, the NaTl structure type may be more stable than the CsCl structure type if the larger atom *M* is highly compressible *and* if the radius ratio of the atoms *M* and *N* is not much larger than unity.[21] Then, atom *M* can be compressed to allow *M*−*N* and *N*−*N* contacts to be established at a smaller average atomic volume than in the CsCl structure type resulting in a lower free energy. These conditions are fulfilled for most of the NaTl type phases containing alkali metals that do not exceed radius ratios larger than 1.15 (see Figure 11). KTl, with a radius ratio of approximately 1.4, is only formed under high pressure.[81] As uranium is not as compressible as the alkali metals – as seen by comparing the bulk modulus of uranium (104 GPa)[64] with the one of potassium

(3 GPa)[82] – the compounds UFe, UCo, UNi, URh, and UIr should also be high-pressure phases as indicated by our calculations (see Section 3.3). In case of the two pseudo-binary alloys $UCo_{0.2}Rh_{0.8}$[78] and $UNi_{0.8}Pt_{0.2}$[79] the pressure is induced chemically by alloying the smaller 3d atoms cobalt and nickel to the larger rhodium and platinum atoms.

After the assumptions of concept of near-neighbor diagrams, Figure 11 reveals that the uranium atoms in the compounds U*T* (*T*: Fe, Co, Ni, Rh, Ir) are successively compressed until *U*–*T* contacts are formed. *T*–*T* contacts are not established in these compounds. These findings are represented in the electron charge density map of hp-UCo shown in Figure 4a. The drawn $(1\bar{1}0)$ plane contains the U–U, U–Co, and Co–Co contact lines. The uranium spheres overlap considerably revealing compressed U–U contacts. The charge density between the uranium and cobalt atoms is polarized towards their contact line representing the U–Co contacts to be formed. The charge density between the cobalt atoms falls rapidly, which is equivalent to the description that Co–Co contacts are not established in hp-UCo.

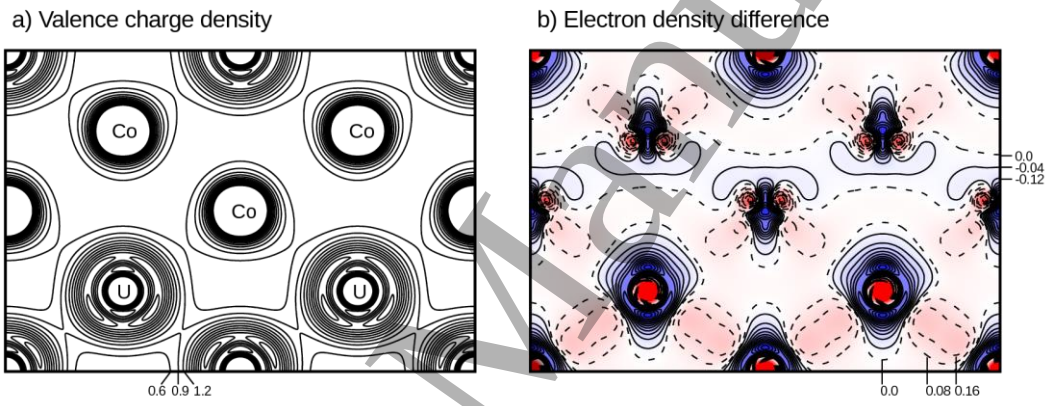

Figure 12: a) Valence electron charge density of hp-UCo in the $(1\bar{1}0)$ plane. Atomic positions are labeled. **b)** Electron density difference ($\rho_{\mathrm{SCF}} - \rho_{\mathrm{atom}}$) map of UCo in the $(1\bar{1}0)$ plane; Density increase: red + dashed line, density decrease: blue + solid line. The shortest interatomic Co–U, U–U, and Co–Co distances are 2.704 Å (PBE/PAW, sp+soc along [001]). The values of the contour lines given are in 10^{-1} (a.u.)$^{-3}$.

Further insight into the bonding interactions of hp-UCo can be achieved by analyzing its electron density difference map as shown in Figure 12b. This kind of map visualizes the difference of the electron density $\rho_{\mathrm{SCF}} - \rho_{\mathrm{atom}}$ after and before the self-consistent field procedure that optimizes the electron density with respect to the total energy. It thus yields information where charge density is enlarged or decreased in the analyzed compound compared to the superposition of free atoms. The charge density difference plot reveals that electronic charge around the uranium atoms is broadly delocalized in the area around the uranium and cobalt atoms reflecting metallic bonding interactions. Figure 12b further shows that electron density is accumulated between the U–U and U–Co contacts. The even distribution between the uranium atoms indicates some amount of covalent bonding, whereas the charge distribution along the U–Co contacts reflects polarized bonding interactions. The

decrease of charge density between the cobalt atoms hints towards nonbonding interactions between these atoms.

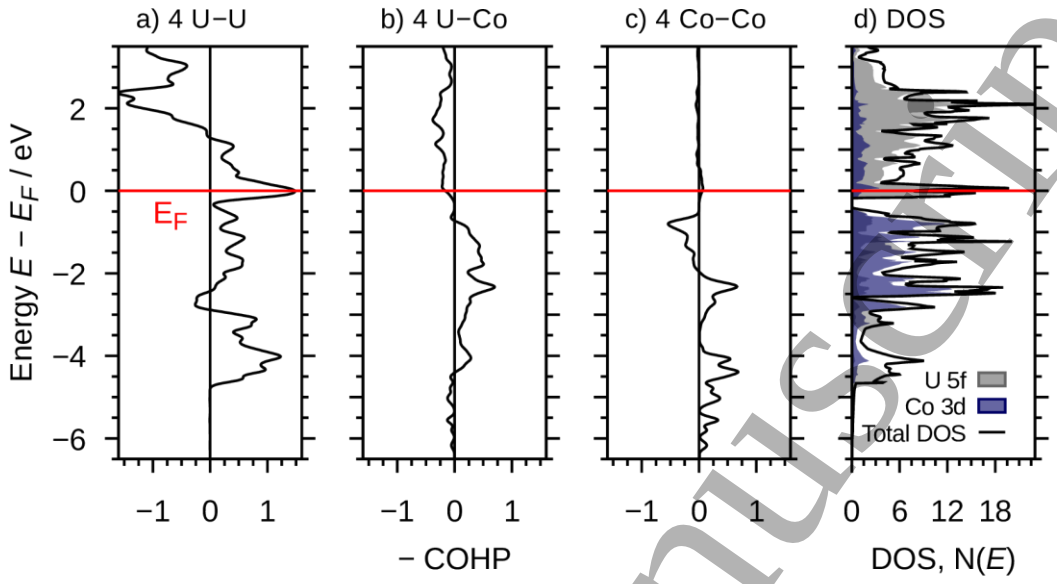

Figure 13: a)-c) COHP analysis of hp-UCo (PBE/PAW). The plots show the COHP contribution for the labeled interactions. **d)** DOS and pDOS of hp-UCo. Overlap of U 5f and Co 3d pDOS are highlighted with a filling with darker color. The calculations were performed without spin-polarization (PBE/PAW).

We performed a Crystal Orbital Hamilton Population (COHP) analysis with no spin-polarization on hp-UCo. The results are displayed in Figure 13a-c. The COHP of the U−U contacts (Figure 13a) displays a strong bonding region ranging from −5 eV to −3 eV and a distinct maximum pinned at the Fermi level. The U−Co interactions result in a broad bonding region from −4 eV to the Fermi level and an antibonding region above E_F corresponding to the overlapping area of the Co 3d-states with the U 5f-states in the DOS. The interactions of the Co 3d-states with each other result in overall nonbonding interactions as shown in Figure 13c. A bonding and an antibonding band is formed between −3.5 eV to −2.0 eV and −2.0 eV to −0.5 eV, respectively. Their bonding and antibonding contributions are of the same amount, thus canceling out in this region. Integrating the COHP curves reveals the four U−U interactions to contribute over 50 % to the total bonding energy of hp-UCo, followed by the four Co−U interactions (20 %) and the four Co−Co interactions (15%). This stresses the importance of the U−U bonding interactions for the overall bond strength of hp-UCo.

4. Summary and Conclusions

In this work, we used evolutionary crystal structure prediction methods combined with DFT calculations to predict a high-pressure phase of the intermetallic compound UCo crystalizing in the

NaTl structure type. Our analysis of the relative stability of this compound applying GGA, LDA, and LDA+*U* calculations reveals that hp-UCo should be stable against decomposition into the adjacent phases UCo_2 and U_6Co and should be formed at pressures below 9 GPa.

Applying the concept of near-neighbor diagrams, our theoretical results are in line with the existing experimental phases. hp-UCo shows the same trends as the two known pseudo-binary compounds $UCo_{0.2}Rh_{0.8}$ and $UNi_{0.8}Pt_{0.2}$. They should be regarded as ordered solid solutions of a bcc lattice following *Vegard's* law. The phase hp-UCo is formed by unfavorably compressing its U−U contacts in agreement to its predicted high-pressure stability. COHP bonding analysis reveals a major contribution of the U−U contacts to the overall bond strength of this phase.

DFT calculations reveal hp-UCo and its related phases UFe and UNi to be magnetic. Their small U−U distances of approximately 2.7 Å are well below the Hill limit. This, as well as the negative dependency of the spin magnetic moments on pressure, characterize these phases as itinerant magnets. In the limit of vanishing spin-orbit interactions UFe and hp-UCo display half-metallic properties: 100 % spin-polarization at the Fermi level E_F. Spin-orbit coupling generally reduces the spin-polarization.

In case of hp-UCo we could show that a subtle interplay of three parameters – the band gap $\Delta_{3d,5f}$, the Stoner exchange integral I_{U5f}, and the magnitude of spin-orbit interactions – can lead to a spin-polarization of more than 90 % at E_F. However, as the applied functionals yield different values for these parameters the prediction of the actual occurrence of half-metallicity in hp-UCo is problematic.

The half-metallic properties of UFe stems from hybridization effects that can be explained in terms of the concept of covalent magnetization. As all tested functionals yield $P(E_F)$ of approximately 90 % for UFe, we think this compound is an even more interesting candidate for half-metallicity than hp-UCo.

Highlighting the close relationship of the NaTl and the MgAgAs structure types, of which the latter contains the first reported half-metallic ferromagnet NiMnSb, we suggest that the space group symmetry of the NaTl structure type promotes the half-metallic properties of UFe and hp-UCo. This makes the NaTl structure type a highly interesting candidate for further investigations on half-metallicity. Against "common sense", we demonstrated that also compounds with heavy elements can show half-metallic properties.

Acknowledgments

We gratefully acknowledge the DFG for funding and the DAAD for travel funding. A.J.K. thanks the Academy of Finland for funding (grant 294799).

References

[1] K.G. Gurtovoi and R.Z. Levitin, Sov. Phys. Uspekhi **30**, 837 (1987).

[2] V. Sechovský and L. Havela, in *Ferromagnetic Materials - A Handbook on the Properties of Magnetically Ordered Substances*, edited by E.P. Wohlfarth and K.H.J. Buschow, 4. (Elsevier Science, Amsterdam, 1988), pp. 309–491.

[3] A.J. Arko, J. Joyce, and L. Havela, in *The Chemistry of the Actinide and Transactinide Elements*, edited by L.R. Morss, N.M. Edelstein, and J. Fuger, 3. (Springer-Verlag, Dordrecht, 2008), pp. 2307–2379.

[4] A.C. Lawson, C.E. Olsen, J.W. Richardson, M.H. Mueller, and G.H. Lander, Acta Crystallogr. B **44**, 89 (1988).

[5] N.C. Baenziger, R.E. Rundle, A.I. Snow, and A.S. Wilson, Acta Crystallogr. **3**, 34 (1950).

[6] T. Siegrist, Y. Le Page, V. Gramlich, W. Petter, A. Dommann, and F. Hulliger, J. Less-Common Met. **125**, 167 (1986).

[7] G. Grübel, J.D. Axe, D. Gibbs, G.H. Lander, J.C. Marmeggi, and T. Brückel, Phys. Rev. B **43**, 8803 (1991).

[8] L. Fast, O. Eriksson, B. Johansson, J.M. Wills, G. Straub, H. Roeder, and L. Nordstrom, Phys. Rev. Lett. **81**, 2978 (1998).

[9] A.T. Aldred, J. Magn. Magn. Mater. **10**, 42 (1979).

[10] A. Dommann, F. Hulliger, and T. Siegrist, J. Magn. Magn. Mater. **67**, 323 (1987).

[11] J.J. Engelhardt, J. Phys. Chem. Solids **36**, 123 (1975).

[12] M.K. Hou, C.Y. Huang, and C.E. Olsen, Solid State Commun. **61**, 101 (1987).

[13] H.R. Ott, H. Rudigier, Z. Fisk, and J.L. Smith, Phys. Rev. Lett. **50**, 1595 (1983).

[14] A. De Visser, A. Menovsky, and J.J.M. Franse, Physica B+C **147**, 81 (1987).

[15] M.B. Maple, J.W. Chen, Y. Dalichaouch, T. Kohara, C. Rossel, M.S. Torikachvili, M.W. McElfresh, and J.D. Thompson, Phys. Rev. Lett. **56**, 185 (1986).

[16] S.S. Saxena, P. Agarwal, K. Ahilan, F.M. Grosche, R.K.W. Haselwimmer, M.J. Steiner, E. Pugh, I.R. Walker, S.R. Julian, P. Monthoux, G.G. Lonzarich, A. Huxley, I. Sheikin, D. Braithwaite, and J. Flouquet, Nature **406**, 587 (2000).

[17] R.A. de Groot, F.M. Mueller, P.G. van Engen, and K.H.J. Buschow, Phys. Rev. Lett. **50**, 2024 (1983).

[18] M.I. Katsnelson, V.Y. Irkhin, L. Chioncel, A.I. Lichtenstein, and R.A. de Groot, Rev. Mod. Phys. **80**, 315 (2008).

[19] W.E. Pickett and H. Eschrig, J. Phys. Condens. Matter **19**, 5203 (2007).

[20] T.B. Massalski, H. Okamoto, and P.R. Subramanian, *Binary Alloy Phase Diagrams*, 2. Edition (ASM International, Ohio, USA, 1990).

[21] W.B. Pearson, *The Crystal Chemistry and Physics of Metals and Alloys* (John Wiley & Sons, Toronto, 1972).

[22] A.R. Oganov and C.W. Glass, J. Chem. Phys. **124**, 4704 (2006).

[23] A.R. Oganov, A.O. Lyakhov, and M. Valle, Acc. Chem. Res. **44**, 227 (2011).

[24] A.O. Lyakhov, A.R. Oganov, H.T. Stokes, and Q. Zhu, Comput. Phys. Commun. **184**, 1172 (2013).

[25] D. Duan, Y. Liu, F. Tian, D. Li, X. Huang, Z. Zhao, H. Yu, B. Liu, W. Tian, and T. Cui, Sci. Rep. UK **4**, 1 (2015).

[26] X. Dong, A.R. Oganov, A.F. Goncharov, E. Stavrou, S. Lobanov, G. Saleh, G.R. Qian, Q. Zhu, C. Gatti, V.L. Deringer, R. Dronskowski, X.F. Zhou, V.B. Prakapenka, Z. Konôpková, I.A. Popov, A.I. Boldyrev, and H.T. Wang, Nat. Chem. **9**, 440 (2017).

[27] A. Bilić, J.D. Gale, M.A. Gibson, N. Wilson, and K. McGregor, Sci. Rep. UK **5**, 1 (2015).

[28] P. Giannozzi et al, J. Phys. Condens. Matter **29**, 1 (2017).

[29] P. Giannozzi et al, J. Phys. Condens. Matter **21**, 1 (2009).

[30] J.P. Perdew, K. Burke, and M. Ernzerhof, Phys. Rev. Lett. **77**, 3865 (1996).

[31] J.P. Perdew and Y. Wang, Phys. Rev. B **45**, 13244 (1992).

[32] P.E. Blöchl, Phys. Rev. B **50**, 17953 (1994).

[33] A.I. Liechtenstein, V.I. Anisimov, and J. Zaanen, Phys. Rev. B **52**, R5467 (1995).

[34] A. Dal Corso, Comp. Mater. Sci. **95**, 337 (2014).

[35] S. Baroni, S. De Gironcoli, A. Dal Corso, and P. Giannozzi, Rev. Mod. Phys. **73**, 515 (2001).

[36] A.A. Mostofi, J.R. Yates, G. Pizzi, Y.-S. Lee, I. Souza, D. Vanderbilt, and N. Marzari, Comput. Phys. Commun. **185**, 2309 (2014).

[37] R. Dronskowski and P.E. Blöchl, J. Phys. Chem. **97**, 8617 (1993).

[38] V.L. Deringer, A.L. Tchougréeff, and R. Dronskowski, J. Phys. Chem. A **115**, 5461 (2011).

[39] S. Maintz, V.L. Deringer, A.L. Tchougréeff, and R. Dronskowski, J. Comput. Chem. **34**, 2557 (2013).

[40] S. Maintz, V.L. Deringer, A.L. Tchougréeff, and R. Dronskowski, J. Comput. Chem. **37**, 1030 (2016).

[41] A.J. Arko, D.D. Koelling, and J.E. Schirber, in *Handbook on the Physics and Chemistry of the Actinides*, edited by A.J. Freeman and G.H. Lander, Vol. 1 (Elsevier, Amsterdam, 1985), pp. 175–238.

[42] P. Söderlind, B. Grabowski, L. Yang, A. Landa, T. Björkman, P. Souvatzis, and O. Eriksson, Phys. Rev. B **85**, 1 (2012).

[43] V.H. Tran and M. Sahakyan, Sci. Rep. UK **7**, 1 (2017).

[44] R. Gumeniuk, A.N. Yaresko, W. Schnelle, M. Nicklas, K.O. Kvashnina, C. Hennig, Y. Grin, and A. Leithe-Jasper, Phys. Rev. B **97**, 1 (2018).

[45] Y. Baer and J.K. Lang, Phys. Rev. B **21**, 2060 (1980).

[46] A.N. Chantis, R.C. Albers, M.D. Jones, M. Van Schilfgaarde, and T. Kotani, Phys. Rev. B **78**, 2 (2008).

[47] H.H. Hill, Nucl. Met. **17**, 2 (1970).

[48] A.G. Petukhov, I.I. Mazin, L. Chioncel, and A.I. Lichtenstein, Phys. Rev. B **67**, 1 (2003).

[49] B. Amadon, Phys. Rev. B **94**, 1 (2016).

[50] B. Himmetoglu, A. Floris, S. De Gironcoli, and M. Cococcioni, Int. J. Quantum Chem. **114**, 14 (2014).

[51] A.B. Shick and W.E. Pickett, Phys. Rev. Lett. **86**, 300 (2001).

[52] J. Rusz and M. Diviš, J. Magn. Magn. Mater. **290–291 PA**, 367 (2005).

[53] W. Xie, W. Xiong, C.A. Marianetti, and D. Morgan, Phys. Rev. B **88**, 235128 (2013).

[54] V.N. Antonov, B.N. Harmon, and A.N. Yaresko, Phys. Rev. B **68**, 1 (2003).

[55] W. Gao, T.A. Abtew, T. Cai, Y.Y. Sun, S. Zhang, and P. Zhang, Solid State Commun. **234–235**, 10 (2016).

[56] P. Janthon, S. Luo, S.M. Kozlov, F. Viñes, J. Limtrakul, D.G. Truhlar, and F. Illas, J. Chem. Theory Comput. **10**, 3832 (2014).

[57] B. Grabowski, T. Hickel, and J. Neugebauer, Phys. Rev. B **76**, (2007).

[58] D. Rappoport, N.R.M. Crawford, F. Furche, and K. Burke, in *Comput. Inorg. Bioinorg. Chem.* (Wiley, Chichester, 2009).

[59] D. van der Marel and G.A. Sawatzky, Phys. Rev. B **37**, 10674 (1988).

[60] A. Debski, R. Debski, and W. Gasior, Arch. Metall. Mater. **59**, 1337 (2014).

[61] H. Fujihisa and K. Takemura, Phys. Rev. B **54**, 5 (1996).

[62] M. Nuding and M. Ellner, J. Alloys Compd. **252**, 184 (1997).

[63] J.P. Itié, J. Staun Olsen, L. Gerward, U. Benedict, and J.C. Spirlet, Physica B+C **139–140**, 330 (1986).

[64] A. Lindbaum, S. Heathman, T. Le Bihan, R.G. Haire, M. Idiri, and G.H. Lander, J. Phys. Condens. Matter **15**, 2297 (2003).

[65] R.F. Zhang, X.F. Kong, H.T. Wang, S.H. Zhang, D. Legut, S.H. Sheng, S. Srinivasan, K. Rajan, and T.C. Germann, Sci. Rep. UK **7**, 1 (2017).

[66] K. Dewhurst, S. Sharma, L. Nordström, F. Cricchio, O. Granas, and H. Gross, http://elk.Sourceforge.net/31.10.2018.

[67] M.I. Aroyo, J.M. Perez-Mato, C. Capillas, E. Kroumova, S. Ivantchev, G. Madariaga, A. Kirov, and H. Wondratschek, Zeitschrift Für Krist. - Cryst. Mater. **221**, 15 (2006).

[68] M.I. Aroyo, A. Kirov, C. Capillas, J.M. Perez-Mato, H. Wondratschek, and IUCr, Acta Crystallogr. Sect. A Found. Crystallogr. **62**, 115 (2006).

[69] P. Mohn, *Magnetism in the Solid State*, 2. edition (Springer-Verlag, Berlin, 2006).

[70] A.R. Williams, R. Zeller, V.L. Moruzzi, C.D. Gelatt, and J. Kubler, J. Appl. Phys. **52**, 2067 (1981).

[71] P. Mohn and K. Schwarz, Physica B+C **130**, 26 (1985).

[72] F. Bultmark, F. Cricchio, O. Grånäs, and L. Nordström, Phys. Rev. B **80**, 035121 (2009).

[73] D. Rappoport, N.R.M. Crawford, F. Furche, and K. Burke, in *Encyclopedia of Inorganic Chemistry*, edited by R.B. King, R.H. Crabtree, C.M. Lukehart, D.A. Atwood, and R.A. Scott (John Wiley & Sons, Ltd, Chichester, UK, 2006), pp. 1–11.

[74] P.J. Hasnip, K. Refson, M.I.J. Probert, J.R. Yates, S.J. Clark, and C.J. Pickard, Philos. Trans. A. Math. Phys. Eng. Sci. **372**, 1 (2014).

[75] P. Villars and K. Cenzual, *Pearson's Crystal Data: Crystal Structure Database for Inorganic Compounds* (ASM International®, Ohio, USA, 2014).

[76] E. Teatum, K. Gschneidner, and J. Waber, *LA-2345* (U.S. Department of Commerce, Washington, D.C., 1960).

[77] A. Simon, Angew. Chem. **95**, 94 (1983).

[78] A.E. Dwight, ANL-7000 **191/5**, (1964).

[79] J.I. Espeso, P. Galez, L. Paccard, C. Lester, D. Paccard, J. Allemand, J.C. Gómez Sal, K.A. McEwen, and K.S. Knight, Solid State Commun. **92**, 389 (1994).

[80] P.C. Schmidt, Struct. Bond. **65**, 91 (1987).

[81] J. Evers and G. Oehlinger, Inorg. Chem. **39**, 628 (2000).

[82] W.R. Marquardt and J. Trivisonno, J. Phys. Chem. Solids **26**, 273 (1965).